Charge ordering on the surface of $Fe_3O_4(001)$

G. Mariotto,* S. Murphy, and I. V. Shvets
SFI laboratories, Physics Department, Trinity College, Dublin 2, Ireland
(Received 11 June 2002; published 31 December 2002)

We have studied the (001) surface of a Fe_3O_4 single crystal using scanning tunneling microscopy (STM), low-energy electron diffraction (LEED), and Auger electron spectroscopy. A clean surface was obtained by a combination of Ar^+ ion sputtering, *in situ* annealing in O_2 atmosphere, and further annealing in ultra high vacuum conditions. A sharp $(\sqrt{2}\times\sqrt{2})R45°$ reconstruction was observed by LEED and STM analysis at room temperature. The STM measurements were performed using a tip of antiferromagnetic MnNi alloy. Atomically resolved STM images provide evidence of a surface terminated at the octahedral plane, with rows of Fe cations running along the [110] and $[1\bar{1}0]$ crystallographic axes. The 3 Å periodicity of the Fe rows expected for a bulk-terminated *B* plane is not observed. Instead, two different kinds of Fe cations with a separation of 6 Å are imaged. The periodicity between Fe cations of the same kind is about 12 Å. We propose a model to explain the observed symmetry in terms of charge ordering of the Fe cations on the octahedral sites of the inverse spinel lattice. We also explain the $(\sqrt{2}\times\sqrt{2})R45°$ LEED pattern in terms of charge ordering, as opposed to a structural rearrangement of the atoms on the surface. We further suggest the possibility of a spin polarized effect, in view of the anomalous corrugation observed along the [110] Fe rows on the octahedral plane, in agreement with the different spin configuration of Fe^{2+} and Fe^{3+} ions.

DOI: 10.1103/PhysRevB.66.245426 PACS number(s): 68.35.Bs, 68.47.Gh, 71.30.+h

I. INTRODUCTION

Spinel ferrites—in the mixed series $M_xFe_{3-x}O_4$, where *M* is a metal—are technologically important materials, with a range of applications including their use in the cores of electromagnets, in microwave resonant circuits, in computer memory cores and in high density magnetic recording media. Magnetite (Fe_3O_4) plays an important role as a catalyst in inorganic processes such as the synthesis of ammonia and the water gas shift reaction for the production of hydrogen, and in organic processes such as the dehydrogenation of ethyl benzene to styrene (see Fig. 1).[1] In the last decade, the great demand for high density magnetic recording media, combined with the possibility of imaging the atomic structure and the electronic properties of the surface provided by scanning tunneling microscopy (STM), has boosted a great interest in magnetite and its related iron oxides. In particular, attention was focused on the study of the surface reconstruction of magnetite and its magnetic properties; the capability of STM to image magnetic surfaces with magnetic contrast down to the atomic scale was demonstrated on the (001) surface of magnetite.[2]

Magnetite is an inverse spinel material. The crystal structure of magnetite is based on a face-centered cubic (fcc) unit cell, containing 32 O^{2-} anions and 24 mixed valence Fe cations, with a lattice parameter of $a=8.3963$ Å.[3] The formula can be written as $Y_A[XY]_BO_4$, where $X=Fe^{2+}$, $Y=Fe^{3+}$, and *A* and *B* denote tetrahedral and octahedral sites, respectively. This formula indicates that one half of the ferric Fe^{3+} ions occupies 8 of the 64 available tetrahedral interstices, and the other half of the ferric ions, together with an equal amount of ferrous Fe^{2+} ions, occupy 16 of the 32 available octahedral interstices. The octahedral planes are separated by an interlayer spacing of 2.1 Å. The nearest-neighbor *B* sites form rows of Fe^{2+} and Fe^{3+} ions running along the [110], $[1\bar{1}0]$, [101], $[10\bar{1}]$, [011], and $[01\bar{1}]$ directions. The rows in alternating octahedral planes are rotated by 90° with respect to one another.

Magnetite undergoes a metal-insulator transition (known as Verwey transition) at around 125 K.[4,5] At room temperature the electrical conductivity of Fe_3O_4 is $\sim 200\ \Omega^{-1}\,cm^{-1}$, but when cooled down below the Verwey transition temperature T_V, the conductivity abruptly decreases by roughly two orders of magnitude.[6,7] The Verwey transition is accompanied by a change in the crystallographic structure, which reduces the symmetry from cubic to monoclinic. This structural transition has been observed by x-ray diffraction[8] and neutron diffraction[9] experiments. The principal axes of the crystal below T_V, *a*, *b*, and *c*, are taken along [110], $[1\bar{1}0]$, and [001] axes of the high-temperature cubic lattice, respectively. Verwey *et al.*[5] first proposed that the transition is due to the ordering of the Fe^{2+} and Fe^{3+} ions on the octahedral sites, and that alternating planes contain either

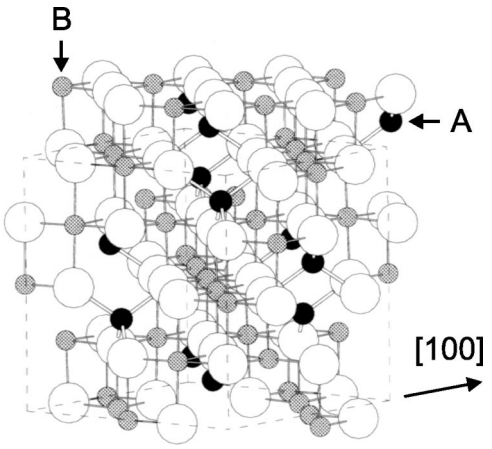

FIG. 1. Model of the magnetite structure. The *A* site and *B* sites in this model are indicated by arrows. The large white spheres indicate the oxygen anions. Reproduced with permission from Ref. 1.

Fe^{2+} or Fe^{3+} only. The low-temperature phase of magnetite has been extensively studied, and several charge-ordering models have been proposed. Shirane *et al.* suggested that every *c* plane contains an equal number of Fe^{2+} and Fe^{3+} ions. Iida *et al.*[10] and Mizoguchi *et al.*[11] based their models on Mössbauer and nuclear magnetic resonance (NMR) experiments and proposed charge ordering models assuming the Anderson condition.[12] Zuo *et al.*[13] studied the ordering of the Fe^{2+} and Fe^{3+} ions on the *B* sites of magnetite below T_V by quantitative high-energy transmission electron diffraction. They found ten independent charge-ordering models for the low-temperature phase that satisfy the Anderson condition[12] if the symmetry is monoclinic. More recently, Kucza[14] analyzed thirty seven configurations allowed by the Anderson condition. Despite the effort, none of the models proposed can explain all the experimental results.

According to the classification of the surfaces of ionic or partly ionic materials given by Tasker,[15,16] the (001) surface of magnetite is polar and therefore must reconstruct or undergo a charge redistribution to minimize the surface energy. A $(\sqrt{2}\times\sqrt{2})R45°$ reconstruction has been observed by other groups both on natural and artificial single crystals,[17,18] and on thin films grown by molecular beam epitaxy (MBE).[19–23] Different models have been proposed to explain this reconstruction, either based on Tasker's electrostatic model[15,16] or on the electron counting model developed by Pashley[24] to explain the reconstructions on compound semiconductors, which was later extended to oxides by Lafemina.[25]

The nature of the termination of the $Fe_3O_4(001)$ surface also remains controversial, as no agreement has been reached on whether a *B*-terminated or an *A*-terminated surface is more favorable. Tarrach *et al.*[17] have suggested that the topmost surface layer consists of a full monolayer (ML) of tetrahedral Fe ions. Such a surface would have an excess electrical charge of $3e^-$ per unit cell. To achieve a non-polar surface they speculated that half of the Fe^{3+} are reduced to $Fe^{0\pm}$. Kim *et al.*[19] have proposed an *A*-terminated surface where the surface charge is autocompensated due to an ordered array of tetrahedral Fe vacancies. More recently, a study by Chambers *et al.*[21] using x-ray photoelectron spectroscopy (XPS), x-ray photoelectron diffraction (XPD), and STM, supports the conclusion that the $Fe_3O_4(001)$ surface is constituted by a half monolayer of tetrahedral Fe. The same model was used by Mijiritskii *et al.*[26] to explain the experimental results obtained using LEED and low energy ion scattering (LEIS) on a thin epitaxial $Fe_3O_4(001)$ film grown by O_2 assisted MBE of Fe on a MgO(001) substrate. Wiesendanger *et al.*[2] imaged two distinct structures on different areas of a natural crystal of magnetite; the two structures were attributed to a tetrahedral and an octahedral termination of the surface, and no reconstruction was observed. In contrast, Voogt *et al.* have proposed a *B*-terminated surface,[27] where autocompensation is achieved by an array of oxygen vacancies accompanied by a variation in the Fe^{3+} to Fe^{2+} ratio per surface unit cell. They speculate that the missing oxygen might act as a $+2$ impurity and could trap conducting electrons from neighboring sites. This would cause a change in the oxidation state of two octahedral iron ions per unit cell from $+2.5$ to $+3$, providing the missing extra electron, necessary to compensate the surface, to the oxygen dangling bonds. A *B*-terminated surface was recently proposed by Stanka *et al.*[28] in a study of epitaxial films of $Fe_3O_4(001)$ grown on MgO (001) substrates in which the $(\sqrt{2}\times\sqrt{2})R45°$ symmetry and the charge balance are achieved by the removal of one oxygen ion per unit cell and by increasing the charge of the octahedral iron ions from $+2.5$ to $+2.7$. Although there is a lack of agreement on the type of surface termination, most groups have explained the $(\sqrt{2}\times\sqrt{2})R45°$ reconstruction in terms of a structural change of the surface, i.e., an ordered array of Fe or O vacancies. In this paper we will present LEED and STM data of a $(\sqrt{2}\times\sqrt{2})R45°$ reconstruction that we explain in terms of charge ordering of the Fe cations at the *B* sites. As pointed out above, both *A*-terminated and *B*-terminated surfaces have been reported in the literature. Stanka *et al.*,[28] for example, have observed an *A*-layer termination on the as-grown surface of a $\sim$5000 Å-thick epitaxial film grown by oxygen-plasma-assisted molecular-beam epitaxy (OPA-MBE) on MgO(001) substrates. Subsequent annealing in oxygen induced a reconstruction that can only be explained in terms of a *B*-terminated surface. These results reveal how critical the preparation conditions of the $Fe_3O_4(001)$ surface are. The *B*-termination showed by our results must then be interpreted in the light of these facts.

II. EXPERIMENTAL

The sample preparation and analysis were performed in a UHV system with a base pressure in the mid 10^{-11} mbar. LEED and AES analysis were performed with commercial retarding-field and cylindrical mirror type analyzers, respectively. STM was performed using a home-built room-temperature instrument, incorporating a piezo tube scanner for tip positioning and a sample approach mechanism similar to that discussed by Mariotto *et al.*[29] All STM images were taken in constant-current mode; the sample was biased and the tip was grounded. A bias voltage ranging from $+0.6$ to $+1$ V and a tunneling current between 0.1 and 0.3 nA were the typical parameters used; scanning with a negative bias was occasionally done, but it did not result in stable tunneling.

The artificial crystal used in this experiments was grown by the skull melting technique.[30] The crystal surface was aligned with a precision of $\pm 1°$ with respect to the (001) crystallographic plane. The crystal was characterized by x-ray diffractometry (XRD) and resistance versus temperature measurements. The diffractograms of a powdered part of the crystal showed good agreement with the data base spectra for magnetite; a lattice constant of 8.40 ± 0.01 Å was measured. Four-wire resistance versus temperature measurements were made between 10 and 300 K on both heating and cooling cycles. A Verwey transition temperature of 108 K was measured, indicating that the composition of the crystal was substoichiometric.

The crystal was mechanically polished using diamond paste with decreasing grain sizes of 3, 1, and 0.25 μm. After polishing, the crystal was cleaned in ethanol using an ultra-

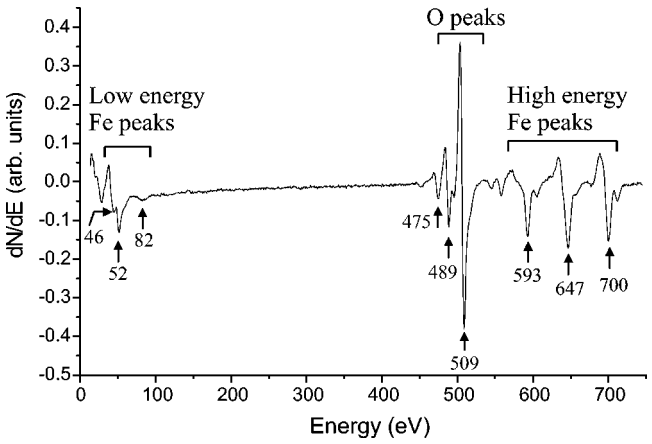

FIG. 2. AES spectrum of a Fe_3O_4 single crystal. No contaminants are detected on the surface. The line shape of the low-energy iron peaks (46 and 52 eV) is in good agreement with that of the reference Auger spectrum of Fe_3O_4 (Ref. 33).

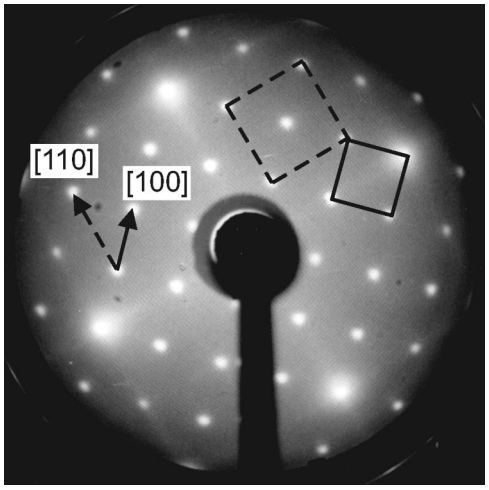

FIG. 3. LEED pattern of a clean $Fe_3O_4(001)$ surface observed with a primary electron energy of 52 eV. A $(\sqrt{2}\times\sqrt{2})R45°$ mesh is visible. The $p(1\times1)$ unit cell and the $(\sqrt{2}\times\sqrt{2})R45°$ superlattice are indicated by a dashed square and a solid square, respectively. The crystallographic axes are marked.

sonic bath. It was then secured onto a Mo sample holder and inserted into the UHV system. The crystal was first prepared in vacuum by means of annealing sessions in UHV at a temperature of 990 ± 50 K for 4–20 h. This method failed to produce a clean surface, and contaminants such as carbon, sulphur, potassium, and calcium were routinely observed. A preparation procedure was then adopted, consisting of a combination of Ar^+ ion sputtering, annealing in UHV and annealing in an oxygen partial pressure. The details of this preparation procedure are described elsewhere.[31] The crystal was annealed in a home-built resistive heater. The temperature was measured by a *K*-type thermocouple spot-welded to a Ta foil placed close to the sample holder. The thermocouple was calibrated to take into account the gradient of temperature from the crystal to the actual point of measurement. The chamber pressure typically remained below 5×10^{-10} mbar while annealing in UHV. This preparation procedure produces a contaminant-free surface, showing a sharp $(\sqrt{2}\times\sqrt{2})R45°$ LEED pattern.

III. RESULTS AND DISCUSSION

A. AES and LEED data

A typical spectrum of the clean surface is shown in Fig. 2, where the contamination levels on the surface are below the detection limit of the analyzer. The preparation procedure used to clean a Fe_3O_4 single crystal surface is critical in determining whether a surface layer that is truly magnetite is obtained, and not a different phase such as maghemite or wüstite. The Fe-O system is complex and the stable phases depend on parameters such as temperature and oxygen content, making the preparation of a clean single crystal surface a difficult task.

The peak shapes of Auger transitions can be used as an indicator of the chemical environment of the various elements comprising the material being probed. As valence band electrons are involved in the transitions, the peak shape of these transitions can be characteristic of the chemical state of the elements. In the case of iron oxides the Fe $M_{2,3}VV$ peak shape is used to determine which iron oxide is present at the surface.[32–35] The line shape of the low-energy iron peaks of the spectrum shown in Fig. 2 is in good agreement with that of the reference Auger spectrum of Fe_3O_4.[33] Two peaks at 46 and 52 eV can be easily identified, the amplitude of the latter being much larger than the former. Such a line shape was found to be highly reproducible every time the crystal's surface was prepared in the fashion discussed above. A different situation arose when the crystal was annealed in UHV for long periods of time. This led to the almost complete disappearance of the 52 eV peak and to an increase of the peak at 47 eV, in agreement with the reference Auger spectrum of wüstite. This result agrees with the expectation that a long annealing under UHV conditions can cause a reduction of the surface from Fe_3O_4 to FeO.

A typical LEED pattern of the surface is shown in Fig. 3. It was taken using a primary electron energy of 52 eV and an emission current of 0.5 mA. Fractional-order spots are clearly visible, indicating that the surface has undergone a $(\sqrt{2}\times\sqrt{2})R45°$ reconstruction. The (1×1) unit cell and the $(\sqrt{2}\times\sqrt{2})R45°$ superlattice are indicated by a dashed and a solid square, respectively. A lattice constant of 8.3 ± 1.7 Å was measured for the conventional unit cell.

B. STM data

All the STM images shown in this paper were taken at room temperature using antiferromagnetic MnNi tips, which were prepared by electrochemical etching in an aqueous solution of (10% volume) saturated HCl and then Ar^+ ion etched in vacuo. A full description of the preparation procedure is given in Ref. 36. Figure 4 shows a (1000×1000) $Å^2$ image in which several terraces are imaged. This type of image has been obtained in numerous STM sessions on a routine basis, using MnNi tips as well as conventional W tips. Two characteristics can be identified from this image:

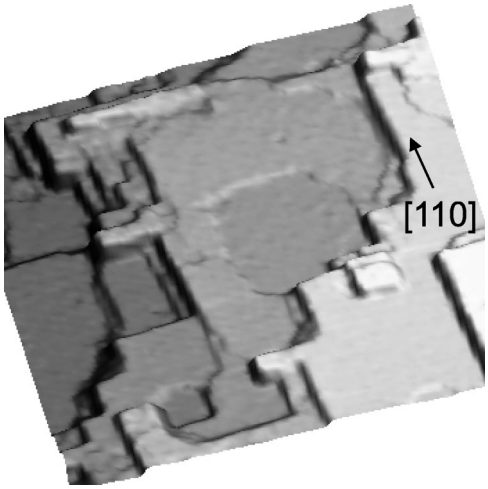

FIG. 4. 3D view of a (1000×1000) Å^2 STM image. The step edge directions lie along the [110] and $[1\bar{1}0]$ crystallographic axes. The step heights are integer multiple of 2.1 Å, which corresponds to the separation between *A*-*A* or *B*-*B* planes. This image was acquired at a positive sample bias voltage of 1.0 V and a tunneling current of 0.1 nA using a MnNi tip.

firstly, the surface edge direction lies along the [110] and $[1\bar{1}0]$ crystallographic axes (as determined from a combination of STM images and LEED data). Secondly, the step heights are an integer multiple of 2.1 Å, which corresponds to the separation between *A*-*A* or *B*-*B* planes. A monoatomic step equal to 1.0 ± 0.1 Å was never observed, ruling out the possibility of both tetrahedral and octahedral atomic planes coexisting on the surface. This result is in agreement with our earlier STM results of $Fe_3O_4(001)$ using nonmagnetic tips.[37] Higher resolution zooms reveal a very sharp and defined atomic structure, as shown in Fig. 5(a). The atomic rows run along the [110] crystallographic axis and are separated by ~6 Å.

Closer inspection of these rows reveals that the corrugation along each row alternates between ''bright points'' of enhanced corrugation, ''dark points'' of lesser corrugation and ''black points'' corresponding to depressions, as shown by the line profile labeled *a*-*a* in Fig. 5(b). For the sake of the argument, from now on we will refer to the two types of protrusions as ''bright points'' and ''dark points,'' and to the depressions as ''black points.'' As we will explain further on, we attribute the bright points and dark points to Fe cations in octahedral coordination and the black points to oxygen anions. The periodicity of the rows along the [110] direction is ~12 Å between points of similar corrugation, and 6 Å between the bright points and dark points; a 3 Å periodicity, as expected for octahedral Fe in bulk magnetite, has never been observed. The periodicity along the [100] direction is ~8.4 Å, in agreement with the values measured from the LEED pattern in Fig. 3. A cubic symmetry is clearly seen on the surface; a black square marked in Fig. 5(a) can be identified with the $(\sqrt{2}\times\sqrt{2})R45°$ reconstructed unit cell (see Fig. 3 for comparison).

The interpretation of STM images in simple geometrical terms—where to each maximum in the tunneling current corresponds one atom—is a simplistic picture and could be erroneous, since the electronic structure contribution can be the predominant one. In the case of transitional metal oxides this was actually found to be the case. Diebold *et al.*[38] have studied the $TiO_2(110)$ surface and have determined that the electronic structure is the dominant factor for the contrast in STM images. A comparison of their experimental data with a theoretical analysis showed that the contrast in their STM images is due to undercoordinated Ti atoms rather than the most exposed oxygen atoms. The predominance of an electronic effect was also observed by Galloway *et al.*[39] on a FeO monolayer grown on Pt(111) where a ''reverse corrugation'' effect has been observed, with the more protruding

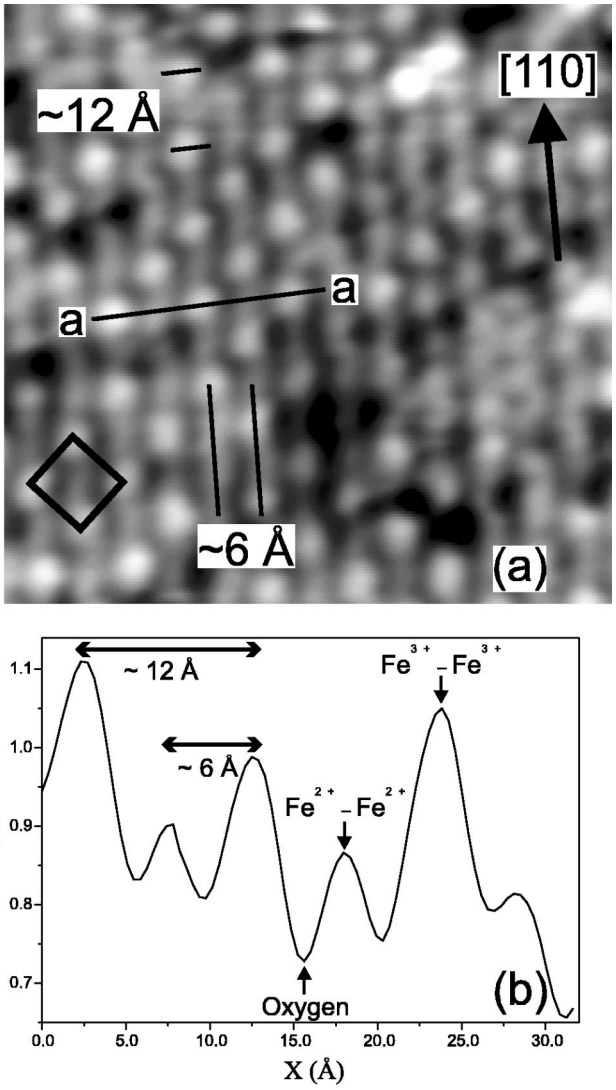

FIG. 5. (a) (70×70) Å^2 STM image. A ~6 Å distance between neighboring rows is observed. The image was acquired at a positive sample bias of 1.0 V and a tunneling current of 0.1 nA using a MnNi tip. (b) Line profile taken along the line labeled $a-a$. The separation between two bright points along the $\langle110\rangle$ directions is ~12 Å; a dark point, at an equal distance of $\sim$ 6 Å between the bright points is revealed by the line profile. We attribute the bright points to Fe^{3+}–Fe^{3+} dimers and the dark points to Fe^{2+}–Fe^{2+} dimers.

sites contributing the least to the average tunneling current. In the case of magnetite, its band structure in the high temperature cubic phase was calculated by Yanase *et al.*[40] They showed that there is a gap in the Fe $3d$ majority spin band at the Fermi level but not in the minority spin band. Moreover, the orbitals just below the Fermi level are composed of $3d$ levels of Fe in the *B* sites. These results are in agreement with the experimental data obtained by Alvarado *et al.*,[41] who measured the spin polarization of photoelectrons from Fe_3O_4. In this work it was shown that electrons from the O $2p$ states lie well below E_F and are therefore not accessible for tunneling experiments. On the basis of these facts, and in agreement with other STM studies of magnetite,[18,28,42] we conclude that STM images of Fe_3O_4 are dominated by Fe cations in *B* sites, which we identify as the bright points and dark points along the atomic rows on the surface in Fig. 5(a).

As stated above, the separation between points of equal corrugation along the [110] direction is $\sim$12 Å, which corresponds to 4 times the distance between Fe cations in octahedral *B* sites in bulk magnetite. The bright points on adjacent rows are shifted in phase by $\sim$6 Å along the [110] direction. The corrugation of the bright points is $\sim$0.2 Å and that of the dark points is $\sim$0.1 Å. A measurement of their full width at half maximum (FWHM) gives an average value of 3 Å. This suggests that Fe^{2+}-Fe^{2+} and Fe^{3+}-Fe^{3+} dimers are imaged, rather than single Fe^{2+} or Fe^{3+} ions. A further argument that the Fe cations imaged by STM lie on the octahedrally coordinated *B* sites is the following. The structure observed, containing an alternating corrugation along the [110]-oriented atomic rows, could not be explained in terms of a tetrahedrally terminated surface, since only one species of Fe cations is present in the *A* sublattice. Even the interpretation of these images in terms of mere topographical contours of the surface would not fit the half-filled *A*-layer model proposed by Kim *et al.*[19] In this case, the 12 Å periodicity between bright points along the [110] direction would be caused by a missing tetrahedral Fe^{3+} per unit cell. The dark points, imaged in the position of the missing tetrahedral ions, should then correspond to Fe ions in octahedral sites and would appear darker because they sit one atomic plane below the surface layer. However, this would not be compatible with the structure of magnetite, since the octahedral ions are not placed exactly under the tetrahedral ones but are shifted by 1.05 Å. No shift is observed in our images. The expected separation along the [110] direction between two adjacent Fe cations in octahedral *B* sites in bulk magnetite is $\sim$3 Å, and such a periodicity has never been observed on any of the images we obtained. Since the Fe^{2+} ions have a larger LDOS than the Fe^{3+} ions and we are probing the empty states, we attribute the bright points to Fe^{3+}-Fe^{3+} dimers and the dark points to Fe^{2+}-Fe^{2+} dimers.

Figure 6 shows a (300×300) Å^2 image where two terraces are separated by 2.1 ± 0.2 Å. A zoom on the terrace, shown by the inset in fig. 6, reveals an atomically resolved structure. The surface structure is identical to the one observed in Fig. 5, with a $\sim$12 Å periodicity measured on the rows along the [110] direction and a separation between adjacent rows of $\sim$6 Å. The shift between two maxima on adjacent Fe rows confirms the $\sim$6 Å value measured on the terrace of Fig. 5. The inset in Fig. 6 shows a dramatic change in the structure observed: atomic resolution is lost in the middle of the image. The loss of atomic resolution is not a sudden change that takes place along a scan line (as marked by the white dashed line in the inset of Fig. 6), and therefore cannot be accounted by a tip change. We speculate that the change resulting in two different domains on the surface may be due to the loss of charge order in the proximity of the terrace edge. The boundary shown by the white dashed line marks the loss of order in the proximity of the terrace step. A possible explanation of this sudden change is a local change in the stoichiometry of the crystal surface. Although our measurements indicate a Verwey transition temperature of 108 K, this value reflects the stoichiometry of the bulk of the crystal. The stoichiometry of the crystal surface is unknown but it is likely to deviate significantly from the value of the bulk, especially considering the preparation procedure employed to prepare the crystal surface in our experiments. We speculate that the areas of the crystal exhibiting long-range order correspond to stoichiometric areas of the surface, and that loss of charge order takes place in off-stoichiometric areas.

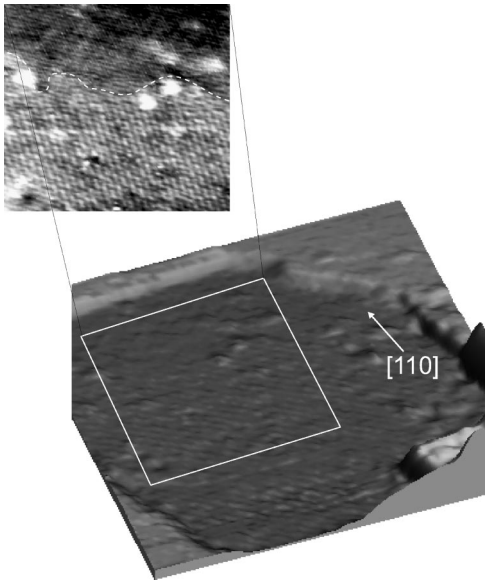

FIG. 6. 3D view of a (300×300) Å^2 STM image. The terrace edge directions lie along the [110] and $[1\bar{1}0]$ crystallographic axes. The two terraces are separated by a 2.1 ± 0.2 Å step height. The inset shows a (170×160) Å^2 zoom. The atomically resolved structure changes in the region marked by the white dashed line. This image was acquired at a positive sample bias voltage of 1.0 V and a tunneling current of 0.1 nA using a MnNi tip.

C. Charge ordering and magnetic contrast

The nature of the Verwey transition[4,5] has been long investigated and, although no definite evidence has been given, it is believed that the transition is due to an ordering of Fe cations in the *B* sites, leading to a reduction in the electrical conductivity. Anderson[12] showed that the repulsion energy due to the cations in octahedral sites is minimized provided

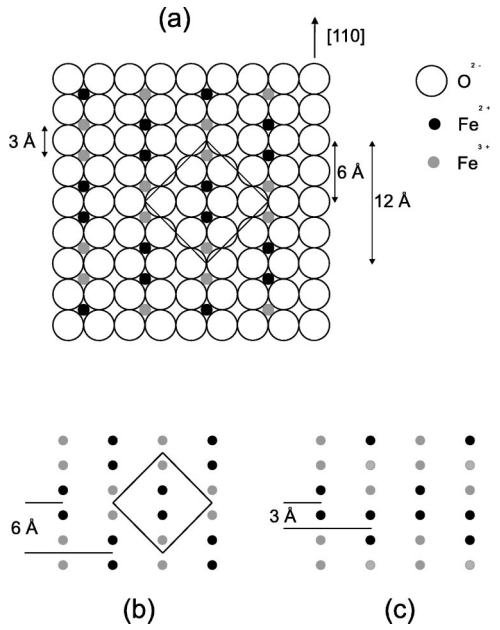

FIG. 7. (a) The (001) surface of Fe_3O_4 terminated at the octahedral plane. The schematic reproduces the structure observed in Fig. 5 (a). Pairs of Fe^{2+} and Fe^{3+} ions run along the [110] direction. The 6 and 12 Å periodicities observed by STM measurements are shown as well as the $(\sqrt{2}\times\sqrt{2})R45°$ reconstruction. (b) and (c) show the comparison between the structure observed by the authors and the one observed by Wiesendanger *et al.*, (Ref. 2) respectively. It can be seen that the shift between pairs of Fe ions of the same type on adjacent rows is 6 Å in our case and 3 Å in Ref. 2. The $(\sqrt{2}\times\sqrt{2})R45°$ reconstruction is indicated in (b).

every tetrahedron formed by the nearest-neighbor octahedral sites is occupied by two Fe^{2+} and two Fe^{3+} ions, imposing the so-called short-range order (SRO). This condition, known as the Anderson condition, can be satisfied by different ionic configurations, which have been extensively discussed.[10,11,13,14]

The results included in this paper provide evidence of charge ordering at the surface of magnetite and of an intimate link between charge ordering and the $(\sqrt{2}\times\sqrt{2})R45°$ mesh observed by LEED and STM. The STM results provide evidence of a highly ordered surface terminated at the octahedral plane. The separation between bright points and dark points, the large value of the FWHM and the difference in corrugation along the [110] directions point to the formation of Fe^{2+}-Fe^{2+} dimers and Fe^{3+}-Fe^{3+} dimers. The symmetry of such a structure is compatible with a $(\sqrt{2}\times\sqrt{2})R45°$ mesh, as shown in Fig. 7(a). We therefore suggest that the superlattice observed by LEED is due to charge ordering on the surface, rather than to a structural change of the surface, such as Fe or O vacancies. The use of electron diffraction as a method to probe charge ordering was proposed by Zuo *et al.*,[13] in virtue of its high sensitivity to the localized outer electrons. Electron diffraction was employed by Rudee *et al.*[43] to analyze charge ordering in Fe_3O_4, supporting the conclusion that the diffraction pattern observed was due to charge ordering.

A $(\sqrt{2}\times\sqrt{2})R45°$ reconstruction has been observed by other groups and different models have been proposed to explain this reconstruction (see Sec. I). Whether the models proposed support a tetrahedral or octahedral termination of the surface, all explain the $(\sqrt{2}\times\sqrt{2})R45°$ reconstruction in terms of structural changes of the surface, with a range of iron and/or oxygen vacancies per unit cell to stabilize the surface energy and to provide the observed surface symmetry. Given the wide range of possible vacancies, the choice of a particular symmetry is to some extent arbitrary. Furthermore, the fractional order spots observed in our LEED pattern are very sharp, suggesting a very well ordered structure. This is supported by the STM images, which show a regular structure—consistent with the $(\sqrt{2}\times\sqrt{2})R45°$ symmetry—on a long-range distance of the order of 40 unit cells. In our view, such a long-range symmetry is better explained by an ordering of electron charges rather than by an ordered array of vacancies. We note that the model we proposed to explain our results leaves the surface not in an autocompensated state. The basic principle of surface autocompensation was postulated by Pashley for semiconductors.[24] It was later extended to oxides by LaFemina.[25] In essence the principle states that a polar surface will reconstruct such that all the anion-derived dangling bonds are full (the oxygen dangling bonds in magnetite) and all the cation-derived dangling bonds are empty (the iron dangling bonds). Recently Kim *et al.*[19] developed a model of the surface of magnetite based on electron counting arguments. Although the model was applied to magnetite in several studies,[19,21,26,28] assumptions about vacancies and redistribution of valence states are made to fit the model to the data. Possibly one could question the universal applicability of the model to the surfaces of oxides and to $Fe_3O_4(001)$ in particular, given that a number of studies show polar surfaces that are not autocompensated. For example, the NiO(111)/NiO(100) system,[44] α-$Fe_2O_3(001)$ under certain preparation conditions,[45–47] $Fe_3O_4(001)$,[2] and other oxides. Yet, our results do not suggest that the autocompensation model should be discarded. It is indeed possible that the surface was not in its ground state, which could explain why it is not in an autocompensated state.

A peculiarity of magnetite resides in its spin electronic band structure. Magnetite has been predicted to be a half-metallic ferrimagnet with a high spin polarization of the electronic states near the Fermi level,[40] and its (001) plane lends itself to magnetic contrast experiments thanks to the different spin configuration of the Fe ions, which is $3d^5$ for Fe^{3+} ions and $3d^6$ for Fe^{2+} ions. Spin polarized STM (SPSTM) uses the spin dependence of the tunneling current to probe the magnetic properties of a sample down to the atomic scale. To achieve magnetic contrast, tip and sample should have a high degree of spin polarization. Different materials, such as ferromagnetic semiconductors, optically pumped semiconductors, ferromagnetic and antiferromagnetic materials have been studied in the past, to produce a tip with such characteristics.

Spin-polarized tunneling was theoretically investigated by Slonczewski[48,49] in the case of a tunnel junction of two fer-

romagnets (f, f') separated by a nonmagnetic barrier b. In a one-dimensional model, in the limit of a free-electron metal at zero temperature, small bias voltage and small barrier transmission, Slonczewski calculated the conductance of the tunnel junction to be

$$G = G_{fbf'}(1 + P_{fb}P_{f'b}\cos\theta), \quad (1)$$

where $G_{fbf'}$ is the mean surface conductance, P_{fb} ($P_{fbf'}$) is an effective spin polarization of the ferromagnet-barrier junction, and θ is the angle between the spin quantization axes of the two ferromagnetic electrodes. Applying this model to an STM tunnel junction, and assuming that the magnetization of the tip and the angle θ between the magnetization of tip and sample are constant, the spin sensitive current representing the local spin direction in the sample and the local magnetic moment can be obtained. Since the magnetic moment of a Fe^{2+} ion is $4\mu_B$ and that of a Fe^{3+} ion is $5\mu_B$, these ions should be distinguishable with a spin-polarized tip.

Magnetic contrast at the atomic level was claimed by Wiesendanger *et al.*[2,50] on the $Fe_3O_4(001)$ surface of a natural single crystal using an Fe tip, and this experiment was recently repeated by Koltun *et al.*[51] on an artificial $Fe_3O_4(001)$ single crystal. A 12 Å periodicity of atomic rows in the octahedral plane was observed. The explanation for this anomalous periodicity, accompanied by a 3 Å shift between maxima on adjacent rows, was based on the theoretical predictions of Iida *et al.*[10] and Kita *et al.*,[52] who studied the possible configurations of Fe^{2+} and Fe^{3+} ions in the low temperature phase of Fe_3O_4, showing that a 12 Å periodicity along the rows of Fe ions at B sites is expected.

Figures 7(b) and 7(c) show the comparison between the structure observed by the authors and the one observed by Wiesendanger *et al.*,[2] respectively. It can be seen that the shift between pairs of Fe ions of the same type on adjacent rows is 6 Å in our case and 3 Å in Ref. 2, leading to a different symmetry of the two structures. The structure shown in Fig. 7(c) would not be in agreement with the $(\sqrt{2}\times\sqrt{2})R45°$ LEED pattern. In addition to the difference in the symmetry of the structure observed, there is a significant difference in the length over which the periodicity is maintained throughout the terrace. In Ref. 50 a quasiperiodicity was observed, with the periods along the rows of iron B sites varying between 6 and 18 Å, although the 12 Å periodicity was the dominant one. On the contrary, what we have imaged is a highly regular structure with a 12 Å periodicity between the same type of Fe ions. Although the Anderson condition stands for bulk magnetite, the structure observed in our STM images is consistent with Andersons's predictions. It shows strong evidence not only of short-range order, but also medium to long range order at the surface of $Fe_3O_4(001)$ at room temperature, giving rise to the formation of a Wigner crystal on the surface due to the localization of the $3d^{\downarrow}$ electrons. The reason for this significant difference is unclear at the moment.

In this paper, the STM measurements of the $Fe_3O_4(001)$ surface were obtained using antiferromagnetic MnNi tips–as suggested by Shvets *et al.*[53]—prepared after Ref. 36. The advantage of using such materials is that they are antiferromagnetic, which eliminates magnetostatic interactions between tip and sample, their mechanical hardness and high Néel temperature. The use of antiferromagnetic tips was first proposed by Minakov *et al.*[54] Using a model of the spin density wave in Cr, it was proposed that antiferromagnetic tips should provide spin contrast. Cr antiferromagnetic tips were successfully used recently[55] to image domains in Fe thin films with a magnetic period of 50 nm.

As discussed in Sec. III B, two different types of Fe ions have been imaged, separated by ~6 Å along the [110] direction, as shown in Fig. 5(a). The line scan in Fig. 5(b) shows a noticeable difference in their corrugation. In the light of charge ordering on the surface, we attributed the bright and dark points to dimers of Fe^{3+} and Fe^{2+} ions forming rows running along the [110] direction. The difference in the corrugation of the dimers may be due to the different LDOS of Fe^{2+} and Fe^{3+} ions. A different mechanism to explain the corrugation change along the [110] rows is a magnetic contrast effect that resolves the different spin configuration of the Fe^{2+} and Fe^{3+} ions. Although our data are not conclusive in this regard, this explanation must be taken into serious consideration since our tip-sample system is capable to provide magnetic contrast, given the electronic properties of magnetite and the use of an antiferromagnetic tip. Experiments with paramagnetic W tips were carried out to clarify whether the contrast observed is due to LDOS or to spin polarization. Although most of the STM sessions were carried out using W tips, we were not able to achieve atomic resolution with such tips and to provide a definite answer.

IV. CONCLUSIONS

We have studied the (001) surface of Fe_3O_4 using a range of surface sensitive techniques such as STM, LEED, and AES. A novel preparation procedure has been developed to prepare a contaminant-free surface of magnetite. A sharp $(\sqrt{2}\times\sqrt{2})R45°$ mesh was observed by LEED and STM analysis at room temperature. We have explained the symmetry observed in terms of charge ordering on the surface of magnetite. We suggest that the origin of the $(\sqrt{2}\times\sqrt{2})R45°$ mesh observed by LEED is due to the charge ordering of the Fe cations in octahedral positions, and not to an ordered array of vacancies as proposed in previous studies. LEED results are in agreement with STM measurements. STM images show an atomic surface arrangement that has never been observed before. Analysis of the STM images leads to the conclusion that the (001) surface of magnetite prepared using our annealing and sputtering routine terminates at the octahedral plane and exposes rows of Fe^{2+} and Fe^{3+} ions in octahedral coordination. Pairs of Fe^{2+} and Fe^{3+} ions on the octahedral plane have been imaged using an antiferromagnetic MnNi tip. The separation between like pairs along the [110] direction is ~12 Å, while pairs of ferrous and ferric cations are separated by ~6 Å. The regular arrangement of the cations pairs is consistent with the $(\sqrt{2}\times\sqrt{2})R45°$ mesh observed by LEED and suggests the onset of charge order at the surface of the crystal at room temperature. A pronounced change in the corrugation of the Fe rows

running along the [110] direction may be interpreted as evidence of a spin polarized effect, reflecting the magnetic contrast due to the different spin configuration of Fe^{2+} and Fe^{3+} ions. Although the presented data are not conclusive, this interpretation cannot be disregarded. We do not suggest that the structure observed by us in this study is the universal structure for the $Fe_3O_4(001)$ surface. It is clear that the structure observed critically depends on the preparation conditions that control the Fe to O ratio on the surface.

ACKNOWLEDGMENTS

The authors would like to thank Professor J.M. Honig for providing the magnetite crystals used in this study. Financial assistance from the Science Foundation Ireland (SFI) agency, Contract No. 00/PI.1/C042, from the EMIT project, Contract No. FMRX-CT98-0198, and from the MAGNETUDE project, Contract No. G5RD-CT-1999-00005, is gratefully acknowledged.

*Email address: mariotl@tcd.ie

[1] R. Cornell and U. Schwertmann, *The Iron Oxides* (Verlagsgellschaft, Cambridge, 1996).
[2] R. Wiesendanger, I. V. Shvets, D. Bürgler, G. Tarrach, H. J. Güntherodt, J. M. D. Coey, and S. Gräser, Science **255**, 583 (1992).
[3] R. W. G. Wyckoff, *Crystal Structures*, 2nd ed. (Interscience, New York, 1964).
[4] E. J. W. Verwey and P. W. Haayman, Physica (Amsterdam) **8**, 979 (1941).
[5] E. J. W. Verwey, P. W. Haayman, and R. Romeyn, J. Chem. Phys. **15**, 181 (1947).
[6] P. A. Cox, *Transition Metal Oxides. An Introduction to their Electronic Structure and Properties* (Clarendon Press, Oxford, 1995).
[7] R. Aragon, R. J. Rasmussen, J. P. Shepherd, J. W. Koenitzer, and J. M. Honig, J. Magn. Magn. Mater. **54-47**, 1335 (1986).
[8] J. Yoshida and S. Iida, J. Phys. Soc. Jpn. **42**, 230 (1977).
[9] M. Iizumi and G. Shirane, Solid State Commun. **17**, 433 (1975).
[10] S. Iida, K. Mizushima, M. Mizoguchi, K. Kose, K. Kato, K. Yanai, N. Goto, and S. Yumoto, J. Appl. Phys. **53**, 2164 (1982).
[11] M. Mizoguchi, J. Phys. Soc. Jpn. **44**, 1501 (1978).
[12] P. W. Anderson, Phys. Rev. **102**, 1008 (1956).
[13] J. M. Zuo, J. C. H. Spence, and W. Petuskey, Phys. Rev. B **42**, 8451 (1990).
[14] W. Kucza, Solid State Commun. **118**, 401 (2001).
[15] P. W. Tasker, J. Phys. C **12**, 4977 (1979).
[16] P. W. Tasker, Philos. Mag. A **12**, 4977 (1979).
[17] G. Tarrach, D. Bürgler, T. Schaub, R. Wiesendanger, and H. Güntherodt Surf. Sci. **285**, 1 (1993).
[18] J. M. Gaines, P. J. H. Bloemen, J. T. Kohlhepp, C. W. T. Bulle-Lieuwma, R. M. Wolf, R. M. Reinders, R. M. Jungblut, P. A. A. van der Heijden, J. T. W. M. van Eemeren, J. aan de Stegge, and W. J. M. de Jonge, Surf. Sci. **373**, 85 (1997).
[19] Y. J. Kim, Y. Gao, and S. A. Chambers, Surf. Sci. **371**, 358 (1997).
[20] S. A. Chambers and S. A. Joyce, Surf. Sci. **420**, 111 (1999).
[21] S. A. Chambers, S. Thevuthasan, and S. A. Joyce, Surf. Sci. **450**, L273 (2000).
[22] Y. Gao and S. A. Chambers, J. Cryst. Growth **174**, 446 (1997).
[23] F. Voogt, Ph.D. thesis, University of Groningen, 1998.
[24] M. D. Pashley, Phys. Rev. B **40**, 10 481 (1989).
[25] J. LaFemina, Crit. Rev. Surf. Chem. **3**, 297 (1994).
[26] A. V. Mijiritskii, M. H. Langelaar, and D. O. Boerma, J. Magn. Magn. Mater. **211**, 278 (2000).
[27] F. C. Voogt, T. Fujii, P. J. M. Smulders, L. Niesen, M. A. James, and T. Hibma, Phys. Rev. B **60**, 11 193 (1999).
[28] B. Stanka, W. Hebenstreit, U. Diebold, and S. A. Chambers, Surf. Sci. **448**, 49 (2000).
[29] G. Mariotto, M. D'Angelo, and I. V. Shvets, Rev. Sci. Instrum. **70**, 3651 (1999).
[30] J. E. Keem, H. R. Harrison, R. Aragon, and J. M. Honig, Inorg. Synth. **22**, 43 (1984).
[31] G. Mariotto, S. Murphy, and I. V. Shvets (unpublished).
[32] M. Seo, J. B. Lumsden, and R. W. Staehle, Surf. Sci. **50**, 541 (1975).
[33] V. S. Smentkowski and J. T. Yates, Surf. Sci. **232**, 113 (1990).
[34] D. Briggs and M. P. Seah, *Auger and X-ray Photoelectron Spectroscopy*, Vol. 1 of *Practical Surface Analysis* 2nd ed. (Wiley, New York, 1990).
[35] C. Ruby, J. Fusy, and J. M. R. Genin, Thin Solid Films **352**, 22 (1999).
[36] S. Murphy, J. Osing, and I. V. Shvets, J. Magn. Magn. Mater. **198-199**, 686 (1999).
[37] C. Seoighe, J. Naumann, and I. Shvets, Surf. Sci. **440**, 116 (1999).
[38] U. Diebold, J. F. Anderson, K.-O. Ng, and D. Vanderbilt, Phys. Rev. Lett. **77**, 1322 (1996).
[39] H. C. Galloway, P. Sautet, and M. Salmeron, Phys. Rev. B **54**, 11 145 (1996).
[40] A. Yanase and K. Siratori, J. Phys. Soc. Jpn. **53**, 312 (1984).
[41] S. F. Alvarado, M. Erbudak, and P. Munz, Phys. Rev. B **14**, 2740 (1976).
[42] J. F. Anderson, M. Kuhn, U. Diebold, K. Shaw, P. Stoyanov, and D. Lind, Phys. Rev. B **56**, 9902 (1997).
[43] M. Rudee, D. Smith, and D. Margulies, Phys. Rev. B **59**, R11 633 (1999).
[44] O. Warren and P. Thiel, J. Chem. Phys. **100**, 659 (1994).
[45] A. Barbieri, W. Weiss, M. V. Hove, and G. Somorjai, Surf. Sci. **302**, 259 (1994).
[46] Q. Guo and P. Moeller, Surf. Sci. **340**, L999 (1995).
[47] N. Condon, F. Leibsle, P. Murray, T. Parker, A. Lennie, D. Vaughan, and G. Thornton, Surf. Sci. **397**, 278 (1998).
[48] J. C. Slonczewski, J. Phys. C **8**, 1629 (1988).
[49] J. C. Slonczewski, Phys. Rev. B **39**, 6995 (1989).
[50] R. Wiesendanger, I. V. Shvets, and J. M. D. Coey, J. Vac. Sci. Technol. B **12**, 2118 (1994).
[51] R. Koltun, M. Herrmann, G. Güntherodt, and V. A. M. Brabers, Appl. Phys. A: Mater. Sci. Process. **73**, 49 (2001).
[52] E. Kita, Y. Tokuyama, A. Tasaki, and K. Siratori, J. Magn. Magn. Mater. **31-34**, 787 (1983).
[53] I. V. Shvets, R. Wiesendanger, D. Bürgler, G. Tarrach, and H. J. Güntherodt, J. Appl. Phys. **71**, 5489 (1992).
[54] A. Minakov and I. Shvets, Surf. Sci. **236**, L377 (1990).
[55] A. Kubetzka, M. Bode, O. Pietzsch, and R. Wiesendanger, Phys. Rev. Lett. **88**, 057201 (2002).